Dentomaxillofacial Radiology (2023) 52, 20230103

birpublications.org/dmfr

RESEARCH ARTICLE

Synthetic MRI for the quantitative and morphologic assessment of head and neck tumors: a preliminary study

[1]Zanxia Zhang, [1]Shujian Li, [1]Weijian Wang, [1]Yong Zhang, [2]Kaiyu Wang, [1]Jingliang Cheng and [1]Baohong Wen

[1]Department of MRI, The First Affiliated Hospital of Zhengzhou University, Zhengzhou, China; [2]MR Research China, GE Healthcare, Beijing, China

Objectives: To evaluate the feasibility of synthetic MRI for quantitative and morphologic assessment of head and neck tumors and compare the results with the conventional MRI approach.

Methods and materials: A total of 92 patients with different head and neck tumor histology who underwent conventional and synthetic MRI were retrospectively recruited. The quantitative T1, T2, proton density (PD), and apparent diffusion coefficient (ADC) values of 38 benign and 54 malignant tumors were measured and compared. Diagnostic efficacy for differentiating malignant and benign tumors was evaluated with receiver operating characteristic (ROC) analysis and integrated discrimination index. The image quality of conventional and synthetic T_1W/T_2W images on a 5-level Likert scale was also compared with Wilcoxon signed rank test.

Results: T1, T2 and ADC values of malignant head and neck tumors were smaller than those of benign tumors (all $p < 0.05$). T2 and ADC values showed better diagnostic efficacy than T1 for distinguishing malignant tumors from benign tumors (both $p < 0.05$). Adding the T2 value to ADC increased the area under the curve from 0.839 to 0.886, with an integrated discrimination index of 4.28% ($p < 0.05$). In terms of overall image quality, synthetic T_2W images were comparable to conventional T_2W images, while synthetic T_1W images were inferior to conventional T_1W images.

Conclusions: Synthetic MRI can facilitate the characterization of head and neck tumors by providing quantitative relaxation parameters and synthetic T_2W images. T2 values added to ADC values may further improve the differentiation of tumors.

Dentomaxillofacial Radiology (2023) **52**, 20230103. doi: 10.1259/dmfr.20230103

Cite this article as: Zhang Z, Li S, Wang W, Zhang Y, Wang K, Cheng J, et al. Synthetic MRI for the quantitative and morphologic assessment of head and neck tumors: a preliminary study. *Dentomaxillofac Radiol* (2023) 10.1259/dmfr.20230103.

Keywords: head and neck tumor; magnetic resonance imaging; synthetic imaging

Introduction

The head and neck is a topographically complex area that is densely populated by vascular and lymphatic structures and vital nerves. Tumor-induced injury to these structures has been associated with significant morbidity and mortality. Diagnosis of soft tissue lesions comprises various pathologic entities commonly located in the mouth, throat, or voice box cancer. Yet, detecting different tumors is sometimes challenging due to the considerable range of morphologic characteristics across different tumor types and within individual tumors.[1] Thus, making an accurate diagnosis is of the utmost importance.

MRI, characterized by excellent soft-tissue contrast and high spatial resolution, has become one of the major modalities used to detect, characterize, grade, or map

Correspondence to: Baohong Wen, E-mail: fccwenbh@zzu.edu.cn

Received 02 March 2023; revised 05 June 2023; accepted 07 June 2023; published online 03 July 2023

The authors Zanxia Zhang and Shujian Li contributed equally to the work.

the extent of head and neck tumors.[2] To date, multiple quantitative MR techniques have been developed, including diffusion-weighted imaging (DWI), intravoxel incoherent motion (IVIM), dynamic contrast-enhanced (DCE) quantitative analysis, and amide proton transfer-weighted (APT) imaging, which have assisted aid preoperative tumor characterization by providing additional information.[3–7] Yet, complex post-processing (especially high variability in clinically used image acquisition and post-processing techniques),[8] low image signal-to-noise ratio,[9] and long scanning time remain the major drawbacks of these methods.[10] The apparent diffusion coefficient (ADC) values, a measure of the magnitude of diffusion of water molecules within tissue, is the most widely used quantitative parameter for differentiating benign and malignant tumors in the head and neck region.[3] However, the ability of ADC values to discriminate between different types of head and neck tumors of different histology is yet to be established.[7]

T1 relaxation, also known as spin lattice or longitudinal relaxation is the time constant used to describe when 63% of the magnetization has recovered to equilibrium. The T2 or transverse relaxation time is related to the lifetime of the magnetization component in the plane perpendicular to the magnetic field direction, which is zero at equilibrium. Proton density (PD) is the most basic MRI measure, representing the apparent concentration of water protons (mobile hydrogen atoms) in each voxel. These measures of a given spin are tissue intrinsic features that only dictated by field fluctuations (both magnetic and electric) that occur in the tissue. So the quantitative T1, T2, and PD values are independent of the MRI equipment or scanning parameters at a given field strength.[11] They provide an absolute scale for the quantitative assessment of tissue properties, allowing for a more objective quantitative analysis of pathophysiological changes in disease.[12] However, the conventional quantitative mapping technique based on a multiecho sequence is unfeasible in clinical practice due to the long acquisition time of the examination. Synthetic MRI is is a novel imaging technique based on multidelay multiecho (MDME) imaging technology that can simultaneously generates both the quantitative maps including T1, T2, and PD and the multiple contrast images, which is beneficial for reducing the acquisition time and avoids spatial mismatch caused by splitting acquisition of different images.[13] The quantitative maps of T1, T2, and PD have been proven of significant advantages in characterizing lesions and monitoring treatment.[14,15] Recent studies have reported preliminary findings of quantitative relaxation parameters generated by synthetic MRI in the brain, breast, prostate, and rectum.[11,16–18] E.g., Gao et al used synthetic relaxometry and diffusion measures for differentiating malignant from benign breast lesions as compared to Breast Imaging Reporting and Data System (BI-RADS), finding lower quantitative T2 and PD values in malignant *vs* benign breast lesions.[17] Moreover, Cui and colleagues assessed quantitative relaxation maps derived from synthetic MRI to diagnose and grade prostate cancer. Diverse T2 values were observed between different grades of prostate cancer and suggested that relaxation maps derived from synthetic MRI may help discriminate malignant lesions from other benign pathologies.[11] Additionally, synthetic MRI can provide synthetic T_1W and T_2W images with comparable contrast to conventional turbo spin echo (TSE) images.[19,20] However, the role of synthetic MRI in head and neck tumors remains unclear.

In this preliminary study, the feasibility of synthetic MRI for the quantitative characterization of head and neck tumors was evaluated and the comparison between these results and ADC values was conducted to determine whether synthetic MRI complements multiplexed sensitivity encoding (MUSE) DWI for tumor characterization. In addition, this study was also aimed to compare the overall image quality of synthetic contrast images with conventional methods (conventional T_1W and T_2W turbo spin echo (TSE) imaging).

Methods and materials

Patients

This retrospective study was approved by the institutional review board of The First Affiliated Hospital of Zhengzhou University. Written informed consent was obtained from all study participants. A total of 112 consecutive patients from The First Affiliated Hospital of Zhengzhou University with pathologically confirmed head and neck tumors were reviewed between May 2022 and November 2022. The inclusion criteria were as follows: (1) no treatment was received before the MR examination; (2) primary tumor >10 mm in size; (3) patients underwent all MRI sequences relevant to the study; (4) patients underwent surgery or biopsy, and the tumor was diagnosed based on the histopathology.

Exclusion criteria were the following: tumor diameter <10 mm; treatment before MR examination;large cystic/necrotic within the tumor; poor image quality; inability to cooperate. The study flow chart is shown in Figure 1.

MR examinations

All patients underwent MR examinations using a 3 T MR scanner (Signa Pioneer, General Electric Healthcare, Milwaukee, WI) with an integrated 19-channel head and neck coil. The patients were scanned in the head-first supine position. Axial T_1 weighted (T_1W) turbo spin echo (TSE) sequence, and axial, coronal, and sagittal T_2 weighted (T_2W) TSE sequences, were first acquired. Thereafter, DWI using multiplexed sensitivity encoding (MUSE) with b values of 0 and 800 s/mm^2 was acquired at the same section position as the axial T_1W. Synthetic MRI was acquired by using a commercially available multidynamic multiecho (MDME) sequence

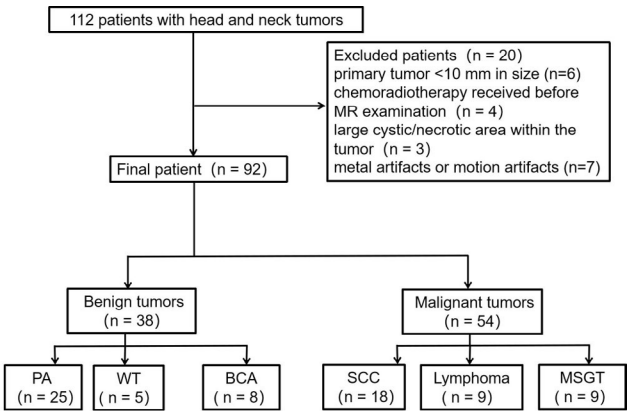

Figure 1 Study flowchart. BCA, Basal cell adenoma; MSGT, malignant salivary gland tumors; PA, Pleomorphic adenoma; SCC, squamous cell carcinoma; WT, Warthin tumor.

with two echo times (13.8/90 ms). The detailed parameters are presented in Table 1.

Quantitative analysis

Data were digitally transferred to the dedicated Advantage Windows workstation (GE Healthcare, AW 4.4). Two radiologists (SJ and WJ, with more than 5 and 8 years of experience in head and neck imaging, respectively) who were blinded to the histopathological results manually drew regions of interest (ROIs) on the relaxation and ADC maps by using the conventional T_2W images for reference. Irregular ROIs were drawn covering the entire tumor (Figure 2), excluding any cystic or necrotic regions. All of the quantitative parameters, including T1, T2, PD, and ADC values, were obtained from the ROIs. The average of the measurements taken by the two radiologists was used for the subsequent analysis. Only the larger lesion was included for analysis for cases with multiple lesions of the same nature. Also, only the primary lesion was included for analysis of cases with primary and nodal diseases in the head and neck region.

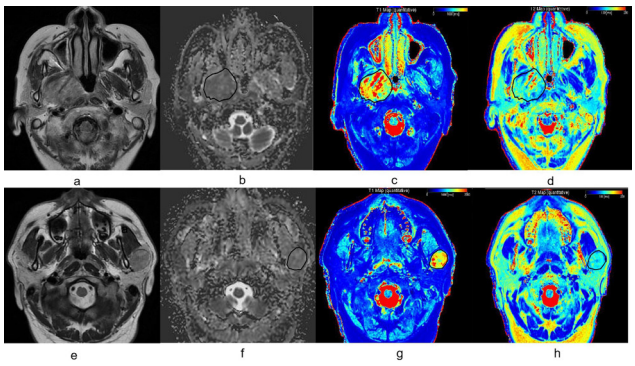

Figure 2 **(a–d)** A 67-year-old patient with oropharyngeal squamous cell carcinoma. **(a)** Axial conventional T_2W)TSE image; **(b)** axial ADC map; **(c)** T1 map; (d) T2 map. **(e–h)** A 27-year-old patient with pleomorphic adenoma in the left parotid gland. **(e)** Axial conventional T_2W TSE image; **(f)** axial ADC map; **(g)** T1 map; **(h)** T2 map. The ROIs were drawn around the tumor on each axial slice to calculate the average value of the whole tumor. The same ROI was duplicated on the same slices of the T1 and T2 map. ADC, apparent diffusion coefficient; ROIs, regions of interest; T_2W, T_2 weighted; TSE, turbo spin echo.

Image quality analysis

Two radiologists (ZX and YZ, with more than 5 and 10 years of experience in head and neck imaging, respectively) independently reviewed synthetic T_1W images, synthetic T_2W images, and the matched conventional images. They were both blinded to the sequence origin and clinical information. The review was conducted for two sessions at a 4-week interval. Each reviewer was given a random set of mixed synthetic T_1W images, synthetic T_2W images, and matched conventional images. The reviewers rated each sequence using a 5-grade Likert scale for overall image quality, where 5 indicated excellent image quality with clear lesion margins without blurring; 4 indicated good image quality with clear lesion margins with mild blurring; 3 indicated moderate image quality with unclear lesion margin with blurring; 2 indicated poor image quality with localized lesion but the indistinguishable shape; 1 indicated unacceptable image quality with unrecognized lesions.

Table 1 MRI acquisition parameters

	Conventional T_1*W TSE imaging*	*Conventional* T_2*W TSE imaging*	*MUSE DWI*	*Synthetic MRI*
TR (ms)	369	4024	3954	4000
TE (ms)	7.8	80	72.7	13.8/90
Field of view (mm^2)	280 × 192	280 × 192	220 × 220	220 × 220
Slice thickness (mm)	4	4	4	4
No. of slices	24	24	24	24
Acquisition matrix	288 × 224	384 × 288	120 × 120	224 × 224
Acceleration factor	2	2	1.5	2.5
b-values (s/mm^2)	NA	NA	0/800	NA
Acquisition time	1 min 33 s	2 min 17 s	1 min 27 s	3 min 28 s

MUSE, mulitiplexed sensitivity encoding; NA, not applicable; TE, echo time; TR, repetition time; TSE, turbo spin echo; T_1W, T_1 weighted; T_2W, T_2 weighted.
[a]

Statistical analyses

IBM SPSS v. 21.0 software (SPSS Inc., Chicago, IL) was used for statistical analyses. The Kolmogorov–Smirnov (K–S) test was used to evaluate the data distribution normality. Differences in the relaxation parameters and ADC values between benign and malignant tumors were compared with the Student's *t*-test or Mann–Whitney *U* test. The receiver operating characteristic (ROC) curves were plotted using MedCalc v. 19.0 (MedCalc Software, Mariakerke, Belgium), and the areas under the curve (AUCs) was calculated to evaluate the diagnostic efficacy of significant relaxation parameters and ADC values for differentiating malignant from benign tumors. The optimal threshold was determined by maximizing the sensitivity plus specificity. The DeLong test was used to compare different AUCs. A one-way analysis of variance (ANOVA) test with Bonferroni correction or Kruskal–Wallis test was conducted to calculate the differences in the relaxation parameters and ADC values between the histologic types of head and neck tumors. The added value of synthetic MRI to DWI was assessed by measuring the integrated discrimination index, as described by Pencina et al.[21] The image quality rating of synthetic images and the matched conventional images were compared using the Wilcoxon signed-rank test. For the quantitative parameters, interobserver agreements were evaluated by using the intraclass correlation coefficient (ICC). Interobserver agreements were evaluated for the image quality rating using the Cohen κ coefficient. A κ/ICC value of 0.21–0.40, 0.41–0.60, 0.61–0.80, and 0.81–1.00 indicated fair, moderate, good, and excellent agreement, respectively. *p*-value <0.05 indicated statistical significance.

Results

A total of 112 patients with head and neck tumors were initially recruited for this study. 20 subjects were excluded from the study due to a tumor diameter <10 mm ($n = 6$), chemoradiotherapy received before MR examination ($n = 4$), large cystic/necrotic area within the tumor ($n = 3$), and metal artifacts or motion artifacts ($n = 7$). The remaining 92 patients with head and neck tumors were enrolled in this study for analysis.

The characteristics of the patients are listed in Table 2. There were 38 benign (25 pleomorphic adenomas, eight basal cell adenomas, and 5 Warthin tumors) and 54 malignant tumors (36 squamous cell carcinomas, 9 lymphomas, and 9 malignant salivary gland tumors). T1, T2, and ADC values were significantly higher in benign tumors than in malignant tumors (Student's *t*-test or Mann–Whitney *U* test: all $p < 0.05$), whereas PD did not differ significantly (Student's *t*-test: $p > 0.05$) (Table 3). The ICC for interobserver agreements showed excellent observer agreement with T1 (0.854), T2 (0.934), and ADC values (0.881) and good agreement for PD (0.798) (Table 3).

Table 2 Characteristics of 92 patients with head and neck tumors

Characteristics	*Finding* (n = *92*)
Age, years (range)	50 (18–77)
Sex	
Male	39
Female	53
Pathology	
Squamous cell carcinoma	36
Lymphoma	9
Malignant salivary gland tumors	9
Mucoepidermoid carcinoma	3
Acinic cell carcinoma	2
Salivary duct carcinoma	2
Adenoid cystic carcinoma	1
Undifferentiated carcinoma	1
Pleomorphic adenoma	25
Basal cell adenoma	8
Warthin tumor	5
Primary tumor location	
Nasopharynx	24
Oropharynx and oral cavity	18
Hypopharynx and larynx	5
Sinonasal region	3
Salivary gland	42

Note: Histological types of lymphoma included 3 diffuse large B cell tumors, 2 Burkitt lymphoma, 2 Hodgkin lymphoma, and 1 MALT lymphoma.

The optimal threshold and AUC of T1, T2 and ADC values in differentiating malignant from benign head and neck tumors are shown in Table 4 and Figure 3. The AUCs of the T2 and the ADC values were 0.752 and 0.839, respectively; however, this difference was not significant (DeLong test: $z = 1.935$, $p > 0.05$). Moreover, the AUCs of ADC and T2 values were higher than that of T1 (DeLong test: $z = 4.341$, $p < 0.05$ and $z = 2.385$, $p < 0.05$, respectively). By adding T2 values to the ADC parameters, the AUC increased from 0.839 to 0.886 with an integrated discrimination index of 4.28%; this improvement was statistically significant (Z test: $p < 0.05$).

The T1, T2, and ADC values showed significant differences among all six groups (ANOVA test or Kruskal–Wallis test: all $p < 0.05$). The analyzed head and neck tumors had a broad range of T1, T2, and ADC values (Tables 5 and 6). The T1 values of Warthin tumors were significantly (Post-hoc test: all adjusted $p < 0.05$) smaller than those of pleomorphic adenomas, lymphoma, and malignant salivary gland tumors. Pleomorphic adenomas had the highest T2 value of 152.00 ± 65.50 ms, which were distinguishable from all other examined types (Post-hoc test: all adjusted $p < 0.05$). Moreover, pleomorphic adenomas had the highest ADC value of $1.70 \pm 0.29 \times 10^{-3}$ mm²/s, which were distinguishable from all other examined types (Post-hoc test: all adjusted $p < 0.05$), and lymphoma had the lowest

Table 3 Relaxation parameters and ADC values of benign and malignant head and neck tumors

Variable	*Benign tumors*	*Malignant tumors*	p-*value*	*ICC (95% confidence interval)*
T1 (ms)	1605.57 ± 554.80	1406.26 ± 199.31	0.004	0.854 (0.709,0.930)
T2 (ms)	132.68 ± 59.81	97.06 ± 12.46	0.000	0.934 (0.709,0.986)
PD (ms)	83.72 ± 7.31	85.33 ± 3.82	0.221	0.798 (0.610,0.901)
ADC ($\times 10^{-3}$ mm²/s)	1.51 ± 0.37	1.05 ± 0.25	0.000	0.881 (0.759,0.943)

ADC, apparent diffusion coefficient; ICC, intraclass correlation coefficient;PD, proton density; SD, standard deviation.
T1, T2 and PD values are derived from synthetic MRI.
Data are mean ± SD.

ADC value of 0.71 ± 0.14×10^{-3} mm2/s, which were distinguishable from all other examined types (Post-hoc test: all adjusted $p < 0.05$).

The image quality scores of the conventional and the matched synthetic contrast images are listed in Table 7. The overall image quality of synthetic T_1W images was statistically inferior to conventional T_1W images for both readers (Wilcoxon signed-rank test; both $p < 0.05$), with a moderate interobserver agreement (κ = 0.471 and 0.512, respectively) (Figure 4). On the other hand, there were no significant differences between the conventional and synthetic T_2W images with regard to overall image quality for both readers (Wilcoxon signed-rank test; both $p > 0.05$) with good interobserver agreements (κ = 0.655 and 0.612, respectively).

Discussion

In the present study, a preliminary investigation was performed utilizing synthetic MRI, including quantitative images (T1, T2, and PD parametric maps) and qualitative morphological images (synthetic T_1W and T_2W images) to characterize head and neck tumors. The results suggested that quantitative T1 and T2 values could be used to differentiate benign and malignant head and neck tumors, and T2 values may add value to ADC values in improving tumor characterization. Additionally, the overall image quality of synthetic T_2W images was comparable to conventional T_2W images.

Relaxation parameters (T1, T2, and PD) can be used to quantify the absolute physical properties of the tissue, thus creating a relationship between MRI images and tissue physiology.[22] In the present study, significant differences were observed in T1 and T2 values, which could be surrogate quantitative imaging biomarkers for free water content and tumor morphology,[23,24] between malignant and benign head and neck tumors; yet, no difference was observed for PD. Consistent with our results for head and neck tumors, T1 and T2 values have been reported to be lower in prostate cancer (lower T1 and T2 values were found in malignant *vs* benign prostate tumors).[11] Increased parenchymal tissue, narrowed extracellular space, and reduced free water content in malignant tumors may cause a decrease in T1 and T2 values.[25] It is worth noting that although the biological behavior of the Warthin tumor is benign, the histology of the Warthin tumor is quite distinct from other benign tumors (pleomorphic adenoma and basal cell adenoma) and has the lowest T1 values. The lowest T1 values were observed for Warthin tumors, which are probably associated with the cystic component in Warthin tumors corresponding to areas with microscopic cysts accumulating proteinous fluid with foamy cells, red cells, and neutrophils.[26] Abundant lymphocytes and lymphoid interstitium in Warthin tumors may also cause a decrease in T1 values. On the other hand, pleomorphic adenomas had the highest T2 values, which may be related to the abundant stroma in mucinous-like tissue, low cell density, and high content of free water molecules.[25] Various proportions of mucinous-like tissue in pleomorphic adenomas may result in a wide span of T2 values. Furthermore, it has been suggested that when mucinous-like tissue occupies a considerable portion of the entire tumor, the envelope of pleomorphic adenoma is thin and prone to rupture, eventually resulting in tumor recurrence.[27] Therefore, T2 values may be a non-invasive marker for the recurrence of pleomorphic adenoma. Moreover, this study indicated that PD values could not be used to differentiate between benign and malignant head and neck tumors. The application of PD in tumor differentiation is relatively rare, probably due to the lack of validated MR sequences to assess PD and the low contrast

Table 4 Diagnostic performance of relaxation parameters and ADC values for differentiating malignant from benign tumors

Variable	*AUC (95% CI)*	*Threshold*	*Sensitivity (%)*	*Specificity (%)*	p-*value*
T1 (ms)	0.617 (0.510–0.717)	≤1688.33	94.44	36.84	0.07
T2 (ms)	0.752 (0.651–0.836)	≤105.17	83.33	63.16	< 0.001
ADC ($\times 10^{-3}$ mm²/s)	0.839 (0.763–0.918)	≤1.18	74.07	84.21	< 0.001
T2 and ADC	0.886 (0.769–0.935)	NA	87.04	80.32	< 0.001

ADC, apparent diffusion coefficient; AUC, area under the receiver operating characteristic curve; CI, confidence interval; NA, not applicable.
T1 and T2 values are derived from synthetic MRI.

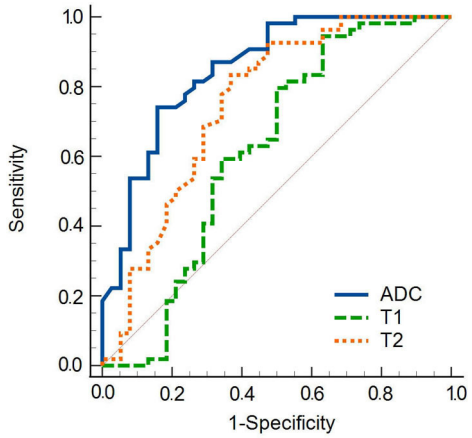

Figure 3 Receiver operating characteristic curves of the T1, T2, and ADC values for distinguishing benign tumors from malignant tumors. ADC, apparent diffusion coefficient.

between benign and malignant tumors in PD-weighted imaging.[17]

Our results showed that ADC values based on DW imaging could be used to distinguish malignant groups from benign head and neck tumors with high diagnostic efficacy. In the comparative analysis of the diagnostic performance of T1, T2, and ADC values for the differentiation of malignant from benign head and neck tumors, the diagnostic efficacy of T2 was lower than the ADC value, but the difference was not statistically significant. The use of any single technique may not be effective in establishing differentiation criteria for head and neck tumors involving different tumor types with different histologies.[5] T2 had lower specificity and accuracy but higher sensitivity than ADC values. Moreover, adding T2 values to the ADC values improved the AUC by up to 0.886 with an integrated discrimination index of 4.28%. These results suggest that T2 values have the potential to provide benign and malignant tumor characteristics that are complementary to the information provided by DWI. This study chose the ADC values as the comparison parameter for quantitative relaxation values, considering that DWI is quite well established as the most successful functional sequence in the head and neck region. Several studies have shown that ADC values can be used to differentiate between benign and malignant head and neck tumors.[28,29] ADC values also showed excellent observer agreements in this study.

In addition to the quantitative analysis of head and neck tumors, the synthetic MRI may also yield synthetic morphological contrast-weighted in one acquisition. Our results indicated that the overall image quality of synthetic T_2W images was comparable to that of conventional T_2W images, and both sequences provided excellent overall image quality. The present finding was consistent with a previous study on rectal cancer,[18] which reported that the image quality of synthetic T_2W images was comparable to that of conventional T_2W images in terms of the SNR, CNR, overall image quality, lesion conspicuity, and absence of motion artifacts. However,

Table 6 *p*-values in the six groups of head and neck tumors

Variable and group	*WT*	*BCA*	*SCC*	*MSGT*	*Lymphoma*
T1 (ms)					
PA	< 0.001	0.081	0.001	0.136	0.289
WT	...	0.111	0.168	0.045	0.016
BCA	...	...	0.420	0.789	0.542
SCC	...	...	...	0.232	0.101
MSGT	...	...	...	...	0.724
T2(ms)					
PA	< 0.001	0.011	< 0.001	0.032	0.007
WT	...	0.068	0.290	0.027	0.067
BCA	...	...	0.170	0.688	0.971
SCC	...	...	...	0.050	0.164
MSGT	...	...	...	...	0.653
ADC ($\times 10^{-3}$ mm^2/s)					
PA	< 0.001	< 0.001	< 0.001	< 0.001	< 0.001
WT	...	0.015	0.124	0.292	0.045
BCA	...	...	0.086	0.092	< 0.001
SCC	...	...	...	0.690	< 0.001
MSGT	...	...	...	...	< 0.001

BCA, basal cell adenoma; MSGT, malignant salivary gland tumors; PA, pleomorphic adenoma; SCC, squamous cell carcinoma; WT, Warthin tumor.
T1 and T2 values are derived from synthetic MRI.

Table 5 Comparison of relaxation parameters and ADC values in the six groups of tumors

Group	*T1 (ms)*	*T2 (ms)*	*PD (ms)*	*ADC ($\times 10^{-3}$ mm^2/s)*
PA (n = 25)	1789.78 ± 562.39	152.00 ± 65.50	91.37 ± 25.71	1.70 ± 0.29
WT (n = 5)	991.31 ± 98.80	85.43 ± 12.49	73.33 ± 5.98	0.96 ± 0.16
BCA (n = 8)	1413.83 ± 322.91	101.83 ± 9.81	82.20 ± 4.33	1.28 ± 0.17
SCC (n = 36)	1374.16 ± 207.01	93.66.51 ± 9.81	84.49 ± 3.25	1.13 ± 0.21
MSGT (n = 9)	1474.07 ± 227.37	106.11 ± 16.84	86.53 ± 3.15	1.09 ± 0.23
Lymphoma (n = 9)	1466.89 ± 100.22	101.63 ± 12.48	87.47 ± 5.51	0.71 ± 0.14
p-value	< 0.001	< 0.001	0.126	< 0.001

ADC, apparent diffusion coefficient; BCA, basal cell adenoma; MSGT, malignant salivary gland tumors; PA, pleomorphic adenoma; PD, proton density ; SCC, squamous cell carcinoma; SD, standard deviation; WT, Warthin tumor.
Data are mean ± SD.
T1, T2 and PD values are derived from synthetic MRI.

Table 7 Qualitative image scores of conventional and the matched synthetic contrast images

Reader	*Conventional* T_1W *images*	*Synthetic* T_1W *images*	p- *value*	*Conventional* T_2W *images*	*Synthetic* T_2W *images*	p-*value*
Reader 1	4.36 ± 0.64	3.68 ± 0.82	< 0.001	4.52 ± 0.54	4.47 ± 0.62	0.102
Reader 2	4.27 ± 0.68	3.78 ± 0.69	< 0.001	4.57 ± 0.54	4.51 ± 0.60	0.083

T_1W, T_1 weighted; T_2W, T_2 weighted.
The image scores are expressed as means ± standard deviations.

the overall image quality of synthetic T_1W images is inferior to that of conventional T_1W images, probably due to the fixed TR/TE combination (TR = 500 ms, TE = 10 ms).[22] Also, the heterogeneity and complexity of the anatomy in the head and neck region and the unaccustomed image contrast can contribute to lower overall image quality scores. Therefore, optimizing parameter combinations based on the specific head and neck region may be necessary.

The present study has a few limitations. First, malignant salivary gland tumors include a variety of tumors with different pathological types. However, the number of tumors in each category was too small for a meaningful comparison of parameter values in each group. Second, our study was limited to the head and neck region, which may influence T1, T2, and PD values, especially in more heterogeneous tumors, such as squamous cell carcinomas. Lastly, all lesions in this study were <10 mm in size; thus, these findings cannot be applied to small tumors.

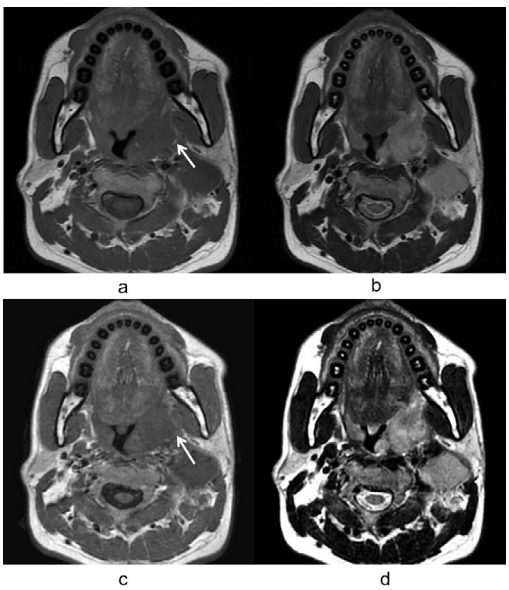

Figure 4 A 30-year-old patient with oropharyngeal squamous cell carcinoma. (a) Axial conventional T_1W TSE image. (b) Axial conventional T_2W TSE image. (c) Synthetic T_1W image. (d) Synthetic T_2W image. Both conventional and synthetic contrast images can clearly display that the tumor was located in the left pharyngeal tonsil; however, the margin of the tumor is blurred on the synthetic T_1W image, and the fatty component of the parapharyngeal space is not as clearly shown as in conventional T_1W images (arrow). T_1W, T_1 weighted; TSE, turbo spin echo.

Conclusion

Our preliminary study demonstrated that T1 and T2 values generated by synthetic MRI might further improve the differentiation between benign and malignant head and neck tumors and different histological types of head and neck tumors. In addition, synthetic T_2W images provided by synthetic MRI techniques showed comparable image quality with the conventional T_2W images, while synthetic T_1W images needed further improvement.

Clinical relevance statement

(1) T1 and T2 values generated by synthetic MRI contribute to the differentiation between benign and malignant head and neck tumors and between different histological types of head and neck tumors.
(2) T2 values can provide information complementary to ADC values provided by diffusion-weighted imaging.
(3) Synthetic T_2W images provided by synthetic MRI techniques have comparable overall image quality to the conventional T_2WI.

Acknowledgements

The authors thank Dr. Lizhi Xie from GE Healthcare for help in solving MR technical problems.

REFERENCES

1. Avey G. Technical improvements in head and neck MR imaging: at the cutting edge. *Neuroimaging Clin N Am* 2020; **30**: 295–309. https://doi.org/10.1016/j.nic.2020.04.002
2. Dai YL, King AD. State of the art MRI in head and neck cancer. *Clin Radiol* 2018; **73**: 45–59. https://doi.org/10.1016/j.crad.2017.05.020
3. Abdel Razek AAK, Gaballa G, Elhawarey G, Megahed AS, Hafez M, Nada N. Characterization of pediatric head and neck masses with diffusion-weighted MR imaging. *Eur Radiol* 2009; **19**: 201–8. https://doi.org/10.1007/s00330-008-1123-6

4. Noij DP, Martens RM, Marcus JT, de Bree R, Leemans CR, Castelijns JA, et al. Intravoxel incoherent motion magnetic resonance imaging in head and neck cancer: A systematic review of the diagnostic and Prognostic value. *Oral Oncol* 2017; **68**: 81–91. https://doi.org/10.1016/j.oraloncology.2017.03.016
5. Sumi M, Nakamura T. Head and neck tumours: combined MRI assessment based on IVIM and TIC analyses for the differentiation of tumors of different histological types. *Eur Radiol* 2014; **24**: 223–31. https://doi.org/10.1007/s00330-013-3002-z
6. Cheng J, Shao S, Chen W, Zheng N. Application of diffusion Kurtosis imaging and dynamic contrast-enhanced magnetic resonance imaging in differentiating benign and malignant head and neck lesions. *Magnetic Resonance Imaging* 2022; **55**: 414–23. https://doi.org/10.1002/jmri.27885
7. Law BKH, King AD, Ai Q-Y, Poon DMC, Chen W, Bhatia KS, et al. Head and neck tumors: amide proton transfer MRI. *Radiology* 2018; **288**: 782–90. https://doi.org/10.1148/radiol.2018171528
8. Keenan KE, Biller JR, Delfino JG, Boss MA, Does MD, Evelhoch JL, et al. Recommendations towards standards for quantitative MRI (qMRI) and outstanding needs. *J Magn Reson Imaging* 2019; **49**: e26–39. https://doi.org/10.1002/jmri.26598
9. Koonjoo N, Zhu B, Bagnall GC, Bhutto D, Rosen MS. Boosting the signal-to-noise of low-field MRI with deep learning image reconstruction. *Sci Rep* 2021; **11**(1): 8248. https://doi.org/10.1038/s41598-021-87482-7
10. Lee EJ, Chang Y-W, Sung JK, Thomas B. Feasibility of deep learning K-space-to-image reconstruction for diffusion weighted imaging in patients with breast cancers: focus on image quality and reduced Scan time. *Eur J Radiol* 2022; **157**: 110608. https://doi.org/10.1016/j.ejrad.2022.110608
11. Cui Y, Han S, Liu M, Wu P-Y, Zhang W, Zhang J, et al. Diagnosis and grading of prostate cancer by relaxation maps from synthetic MRI. *J Magn Reson Imaging* 2020; **52**: 552–64. https://doi.org/10.1002/jmri.27075
12. Hagiwara A, Hori M, Yokoyama K, Takemura MY, Andica C, Kumamaru KK, et al. Utility of a Multiparametric quantitative MRI model that assesses myelin and edema for evaluating plaques, Periplaque white matter, and normal-appearing white matter in patients with multiple sclerosis: A feasibility study. *AJNR Am J Neuroradiol* 2017; **38**: 237–42. https://doi.org/10.3174/ajnr.A4977
13. Ji S, Yang D, Lee J, Choi SH, Kim H, Kang KM. Synthetic MRI: technologies and applications in Neuroradiology. *J Magn Reson Imaging* 2022; **55**: 1013–25. https://doi.org/10.1002/jmri.27440
14. Adams LC, Bressem KK, Scheibl S, Nunninger M, Gentsch A, Fahlenkamp UL, et al. Multiparametric assessment of changes in renal tissue after kidney transplantation with quantitative MR Relaxometry and diffusion-Tensor imaging at 3 T. *J Clin Med* 2020; **9**(5): 1551. https://doi.org/10.3390/jcm9051551
15. Du S, Gao S, Zhao R, Liu H, Wang Y, Qi X, et al. Contrast-free MRI quantitative parameters for early prediction of pathological response to Neoadjuvant chemotherapy in breast cancer. *Eur Radiol* 2022; **32**: 5759–72. https://doi.org/10.1007/s00330-022-08667-w
16. West H, Leach JL, Jones BV, Care M, Radhakrishnan R, Merrow AC, et al. Clinical validation of synthetic brain MRI in children: initial experience. *Neuroradiology* 2017; **59**: 43–50. https://doi.org/10.1007/s00234-016-1765-z
17. Gao W, Zhang S, Guo J, Wei X, Li X, Diao Y, et al. Investigation of synthetic Relaxometry and diffusion measures in the differentiation of benign and malignant breast lesions as compared to BI-RADS. *J Magn Reson Imaging* 2021; **53**: 1118–27. https://doi.org/10.1002/jmri.27435
18. Zhao L, Liang M, Wu PY, Yang Y, Zhang H, Zhao X. A preliminary study of synthetic magnetic resonance imaging in Rectal cancer: imaging quality and preoperative assessment. *Insights Imaging* 2021; **12**(1): 120. https://doi.org/10.1186/s13244-021-01063-w
19. Tanenbaum LN, Tsiouris AJ, Johnson AN, Naidich TP, DeLano MC, Melhem ER, et al. Synthetic MRI for clinical neuroimaging: results of the magnetic resonance image compilation (magic) prospective, multicenter, Multireader trial. *AJNR Am J Neuroradiol* 2017; **38**: 1103–10. https://doi.org/10.3174/ajnr.A5227
20. Yi J, Lee YH, Song HT, Suh JS. Double-inversion recovery with synthetic magnetic resonance: a pilot study for assessing Synovitis of the knee joint compared to contrast-enhanced magnetic resonance imaging. *Eur Radiol* 2019; **29**: 2573–80. https://doi.org/10.1007/s00330-018-5800-9
21. Pencina MJ, D'Agostino RB, D'Agostino RB, Vasan RS. Evaluating the added predictive ability of a new marker: from area under the ROC curve to reclassification and beyond. *Stat Med* 2008; **27**: 157–72. https://doi.org/10.1002/sim.2929
22. Konar AS, Paudyal R, Shah AD, Fung M, Banerjee S, Dave A, et al. Qualitative and quantitative performance of magnetic resonance image compilation (magic). *Method: An Exploratory Analysis for Head and Neck ImagingCancers (Basel)* 2022; **14**: 3624. https://doi.org/10.3390/cancers14153624
23. McSheehy PMJ, Weidensteiner C, Cannet C, Ferretti S, Laurent D, Ruetz S, et al. Quantified tumor T1 is a generic early-response imaging biomarker for chemotherapy reflecting cell viability. *Clin Cancer Res* 2010; **16**: 212–25. https://doi.org/10.1158/1078-0432.CCR-09-0686
24. Li S, Liu J, Zhang F, Yang M, Zhang Z, Liu J, et al. Novel T2 mapping for evaluating Cervical cancer features by providing quantitative T2 maps and synthetic morphologic images: A preliminary study . *J Magn Reson Imaging* 2020; **52**: 1859–69. https://doi.org/10.1002/jmri.27297
25. Baohong W, Jing Z, Zanxia Z, kun F, Liang L, Eryuan G, et al. T2 mapping and Readout Segmentation of long variable echo-train diffusion-weighted imaging for the differentiation of Parotid gland tumors. *European Journal of Radiology* 2022; **151**: 110265. https://doi.org/10.1016/j.ejrad.2022.110265
26. Ikeda M, Motoori K, Hanazawa T, Nagai Y, Yamamoto S, Ueda T, et al. Warthin tumor of the Parotid gland: diagnostic value of MR imaging with histopathologic correlation. *AJNR Am J Neuroradiol* 2004; **25**: 1256–62.
27. Prades J-M, Oletski A, Faye M-B, Dumollard J-M, Timoshenko A-P, Veyret C, et al. Parotid gland masses: diagnostic value of MR imaging with histopathologic correlations. *Morphologie* 2007; **91**: 44–51. https://doi.org/10.1016/j.morpho.2007.05.003
28. Norris CD, Quick SE, Parker JG, Koontz NA. Diffusion MR imaging in the head and neck: principles and applications. *Neuroimaging Clin N Am* 2020; **30**: 261–82. https://doi.org/10.1016/j.nic.2020.04.001
29. El Beltagi AH, Elsotouhy AH, Own AM, Abdelfattah W, Nair K, Vattoth S. Functional magnetic resonance imaging of head and neck cancer: performance and potential. *Neuroradiol J* 2019; **32**: 36–52. https://doi.org/10.1177/1971400918808546